



Contents lists available at ScienceDirect

Journal of Marine Systems

journal homepage: www.elsevier.com/locate/jmarsys

Reconstruction of the Mediterranean northern current variability and associated cross-shelf transport in the Gulf of Lions from satellite-tracked drifters and model outputs

A. Rubio ^{a,*}, V. Taillandier ^b, P. Garreau ^c

^a IFREMER, Centre de Méditerranée, B.P. 330, 83500 La Seyne sur Mer, France

^b LOCEAN, Paris, France

^c IFREMER, Centre de Brest, Plouzané, France

ARTICLE INFO

Article history:

Received 10 December 2007

Received in revised form 27 May 2008

Accepted 22 January 2009

Available online xxx

Keywords:

Lagrangian data
Flow reconstruction
Shelf-slope transport
Coastal circulation
Mesoscale variability
Mesoscale eddies
Slope current

ABSTRACT

The reconstruction of currents at 50 m depth was performed in the Gulf of Lions, merging Lagrangian data with outputs from a numerical ocean model. The Lagrangian data set consists of trajectories obtained from 12 satellite-tracked drifters released in the Northern Current in June 2005. The low-pass filtered trajectories revealed the well-known mean patterns of along-slope circulation and sampled its mesoscale activity, showing meandering pathways over the slope and closed pathways trapped over the shelf. They were used to reorganise the model eddy activity by refining the location and shape of meanders and eddies. The impacts of the reconstruction procedure were assessed by comparing the simulated and reconstructed fields with simultaneous SST images. Finally, the reconstructed fields were used to study some of the observed mesoscale structures. They provide a realistic scenario for diagnostics of the shelf-slope transports in the Gulf of Lions.

© 2009 Elsevier B.V. All rights reserved.

1. Introduction

In the north-western basin of the Mediterranean Sea, the Gulf of Lions is a region of special interest (Fig. 1a). This coastal shelf is characterised by a complex circulation pattern resulting from direct and indirect effects of intense local forcings (namely north and north-westerly winds and the Rhone river's inputs). Moreover, the Gulf of Lions is largely open to regional circulation with a strong geostrophic current called the Northern Current (hereinafter referred to as NC). The NC flows cyclonically along the gulf, bordering the slope over the 1000–2000 m isobaths (Millot, 1990; Conan and Millot, 1995). This current can drastically influence gulf shelf dynamics and play an important role in exchanges between coastal and marine waters. The NC is affected by a large spectrum of variability. Seasonal variations of its mean shape have been extensively observed, with the current becoming narrower, deeper and more intense during wintertime (Millot, 1999). The NC's mesoscale activity is also noticeable, in the form of intense meanders, filaments and eddies. Its meandering features can develop and propagate along its whole pathway (Millot,

1990; Sammari et al., 1995; Alberola et al., 1995; Flexas et al., 2002; Rubio et al., 2007). Such instabilities are driven by the combination of barotropic processes, related to horizontal shear perturbations, and baroclinic processes, related to major changes of the stratification (Crépon et al., 1982; Sammari et al., 1995; Flexas et al., 2002, 2005). The mesoscale variability of the NC can significantly impact shelf water renewal and the activity of the local ecosystem (e.g., Durrieu de Madron et al., 1999).

In this context, an observation system based on satellite-tracked Lagrangian drifters was set up in June 2005 for the monitoring of subsurface circulation along the Gulf of Lions shelf slope (project ECOLOPHY; see <http://www.ifremer.fr/sismer/UK/catal/campagne/campagnea.html?crno=5450150> and André, 2007). These drifters were anchored at a depth of 50 m to ensure that they move in good approximation with the circulation below the Ekman layer. Regularly deployed at the core of the NC upstream of the Gulf of Lions, the drifters sampled the variability of some dynamic characteristics of the NC over several weeks. In particular, position data collected in real time provided direct information about the underlying velocity field and associated transport.

This is not the first time that Lagrangian data have been used to investigate hydrodynamic processes in Mediterranean coastal zones (Poulain, 2001; Salas et al., 2002; Testor and Gascard, 2003; Veneziani et al., 2007). It is well known that Lagrangian data sets have greatly contributed to our knowledge of coastal circulation worldwide in

* Corresponding author. Current address: AZTI-Tecnalia Marine Research Division, Pasaia (Gipuzkoa), Spain.

E-mail addresses: arubio@azti.es (A. Rubio), vta@locean-ipsl.upmc.fr (V. Taillandier), pierre.garreau@ifremer.fr (P. Garreau).

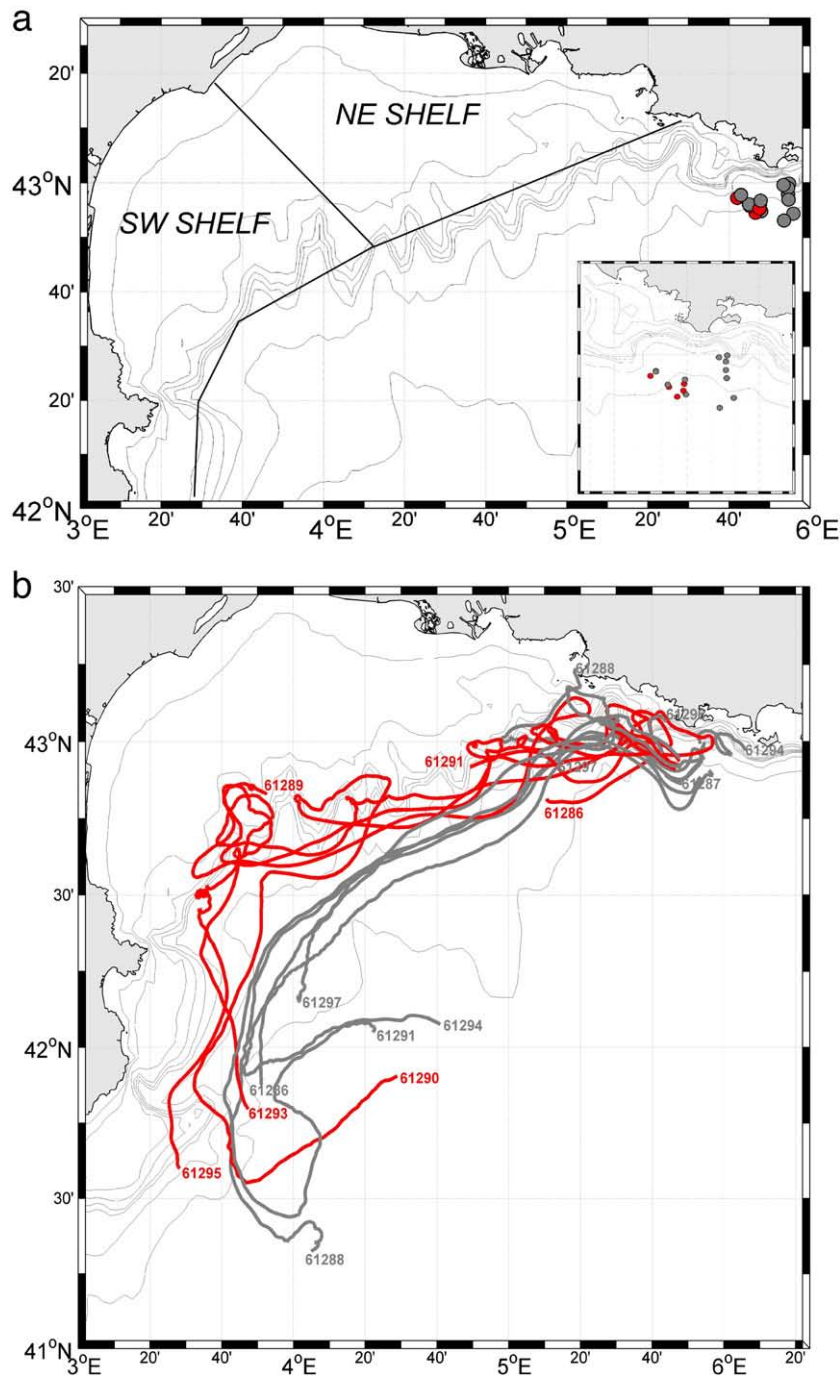


Fig. 1. a) Bathymetry of the Gulf of Lions (isobaths: 50, 100, 200, 300, 400, 500, 1000 and 2000) and June 2005 drifter deployment points. The shelf zones defined for diagnostic purposes (Section 5) are delimited by black solid lines. b) Low pass filtered trajectories in the NW Mediterranean (isobaths: 50, 100, 200, 300, 400, 500, 1000 and 2000) for June 2005 drifter deployment. The 6 trajectories used for the reconstruction of the Eulerian fields are plotted in red.

terms of mean flow and variability (Davis, 1991). Recently, growing attention has been given to using Lagrangian data in operational mode in order to provide Rapid Environmental Assessments (REA). They now appear to be of prime importance in many related applications, such as search and rescue, forecasting and containment of pollutants, and mine warfare (e.g., Rixen and Ferreira-Coelho, 2007; Rixen et al., 2008). They have also led to challenging methodological developments in reconstructing of flows observed from drifter trajectories (Özgökmen et al., 2000; Toner et al., 2001; Castellari et al., 2001; Molcard et al., 2003; Taillandier et al., 2006) as well as in assimilating them to improve the realism of modelling and forecasting platforms

(Kamachi and O'Brien, 1995; Özgökmen et al., 2003; Kuznetsov et al., 2003; Taillandier and Griffa, 2006).

In accordance with these developments, position data obtained from the set of drifters released in the Gulf of Lions were combined with MARS3D hydrodynamic model (Lazure and Dumas, 2008) outputs to obtain the best representation of shelf-slope circulation over a 6 week period (starting at the end of June 2005). Ideally, state-of-the-art models with resolution on the order of a few kilometres (like the one considered here), could resolve almost all the NC's variability, except for submesoscale turbulence which is expected to be only partially resolved. In practice, there are a number of issues in addition to spatial and

temporal resolution that introduce additional model errors and further limit this capability (i.e., incomplete knowledge of forcings, limitations in resolved physics). Merging model outputs and Lagrangian data is expected to improve model simulations of NC variability. Moreover, it provides a targeted analysis of the Lagrangian database within given scales of variability.

To combine Eulerian model fields and Lagrangian data, we applied an inverse method previously developed by Taillandier et al. (2006). The methodology's influence was assessed by qualitative comparison between the reconstructed fields and independent data from satellite thermal images. Then, quantities characterising the cross shelf transports inferred by the NC mesoscale variability and the residence times over the shelf were closely examined. The present application to NC dynamics demonstrated its capacity for monitoring and Rapid Environmental Assessments.

This paper is organised as follows: the material used to observe NC mesoscale variability during summer 2005 is presented in Section 2. The modelling and reconstruction methodology are described in Section 3, along with the Lagrangian diagnostics performed on model outputs. The parameterisation for reconstruction and its implementation on observations and model outputs are described in detail in Section 4. Results obtained from the reconstruction are presented in Section 5. Finally, the summary and concluding remarks are given in Section 6.

2. Material

2.1. Satellite-tracked drifters

12 drifting buoys were tracked by the ARGOS satellite system in the north-western Mediterranean Sea during summer 2005. These (WOCE type) instruments were basically composed of a spherical float ~40 cm in diameter and a 10 m long holey-sock drogue. The surface float contained a thermistor to measure temperature (30 cm beneath the sea surface) and a submergence sensor to verify the presence of the holey-sock drogue. For this experiment, the drogue was centred 50 m below the surface so that buoys could be considered to be drifting in good approximation with shelf-slope dynamics underneath the Ekman layer. Moreover, the drogue was also centred at 50 m to allow the buoys to drift freely over the deeper part of the Gulf of Lions shelf (it is worth noting that the length of the drifting instrument is around 60 m, as there is a supplementary weighted chain at the end of the holey-sock drogue).

Drifters were deployed in pairs at the south-eastern part of the Gulf of Lions (Fig. 1a). The first deployment was performed between 29

May and 2 June 2005. Then a second deployment, reusing 6 of the drifters (recovered on the coast) was carried out on 3 July 2005. Both deployments were done within an approximately 15 km square cluster covering the core vein of the NC (Fig. 1a). Position, temperature and submergence data were collected and transmitted almost every hour during the whole summertime period. A Lagrangian dataset of 18 trajectories in all was compiled from the drifter measurements. To do so, the position data were processed in the following way. First, a simple criterion applied along each trajectory aimed at removing outliers: the misfit between Lagrangian velocities and their statistic mean was computed over running windows of 20 positions in order to reject values which differ from the mean by more than three times the standard deviation. Secondly, the presence of the holey-sock drogue was checked using submergence values. When their anchor is lost, drifters can be directly influenced by wind and waves, so that trajectory information becomes less consistent with the circulation under the Ekman layer. The submergence sensor provides indirect information about the presence or absence of the holey sock drogue. When the drogue is anchored, submergence episodes are frequent due to the vertical strain caused by the drogue. When the drogue is lost submergence rarely occurs. This indicator can be quite inaccurate, which is why the submergence sensor information was checked by visual validation of the trajectories, especially under strong wind conditions when it was easy to check whether or not the buoys had followed the direction of the surface wind field. In the third step, positions were interpolated at a 1 h-resolution using a piecewise cubic scheme to obtain regular time series. Then, a Butterworth low-pass filter with a cut-off period of 18 h was applied to derived Lagrangian velocities in order to remove HF signals mainly related to inertial oscillations. Finally, the trajectories obtained were sub-sampled at a 3 h-resolution. Low-pass filtered trajectories corresponding to buoys with the holey-sock drogue are shown in Fig. 1b.

Trajectories revealed the well-known mean patterns of along-slope circulation in the Gulf of Lions. Drifters launched from 29 May–2 June showed intense NC meandering and most of them left the current in their path along the slope to circulate in mesoscale structures over the shelf (Fig. 1b). Conversely, trajectories corresponding to the second deployment (3 July), whose drift followed the offshore part of the slope current vein, did not show this meandering and presented much less variability. Finally, it is worth noting the behaviour of the drifters in the southern part of the gulf: all the drifters which keep their holey sock drogue left the slope current around 41.7° , circulating cyclonically towards the open sea. From the combined analysis of trajectories and available SST satellite images (not shown), it appears that the buoys' paths coincided with the presence of a strong surface

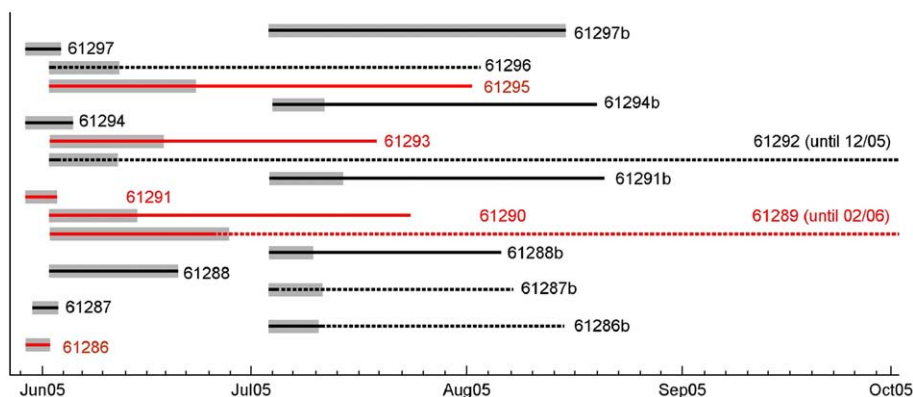


Fig. 2. Buoy lifetimes. Solid lines indicate trajectories corresponding to drifters with the holey-sock drogue and dashed lines to those drifters which had lost the holey-sock drogue. Grey thick lines indicate the time that buoys remained in the Gulf of Lions (time before crossing the latitude 42°). The 6 trajectories used for the reconstruction of the Eulerian fields are plotted in red.

thermal front showing the southern limit of the Gulf of Lions cold waters (Lopez-Garcia et al., 1994).

Drifter lifetimes lasted from a few days to some months, with a mean lifetime equal to 54 days (Fig. 2). The drogue was lost before the death of the buoy in 45% of cases, making a mean lifetime of the holey sock drogue of around 24 days. The maximum spatial-temporal coverage was reached in the north-eastern part of the Gulf of Lions and over the shelf slope (grey shade in Fig. 2), where most drifters remained at the NC's core during several days after their deployment.

2.2. SST imagery

Three SST images were used over the Gulf of Lions on 19 and 29 June and 5 July 2005. They were provided by the French NAUSSICA (IFREMER <http://www.ifremer.fr/nausicaa/rozes/index.htm>) and the Spanish SAIDIN (CMIMA-CSIC, <http://ers.cmima.csic.es/saidin>) databases. It should be noted that this synoptic information was not compared with the temperature data acquired by the drifters. The thermal fronts described by IR imagery were only used to document the location and shape of the NC over the shelf slope in qualitative terms. The contrast between marine waters carried by the NC and coastal waters over the gulf characterised meanders and eddies of the surface circulation (Sammari et al., 1995; Flexas et al., 2002; Rubio et al., 2005).

3. Numerical tools

3.1. Realistic modelling

Modelling was performed using MARS3D (3D hydrodynamic Model for Applications at Regional Scale, IFREMER), a 3D primitive equation free surface model subjected to the Boussinesq and

hydrostatic approximation (see a detailed description in Lazare and Dumas, 2008). Spatial discretisation was done using a staggered “C” grid (Arakawa and Lamb, 1977) and vertical sigma-coordinates. For this study, MARS3D was used in its configuration for the NW Mediterranean (MENOR) with a horizontal resolution of 1.2 km and 30 sigma layers. The entire model domain covers the area east of Corsica and Sicily, the Ligurian Sea, Gulf of Lions and the Catalan Sea to the north of the Balearic Islands, which was the zone of interest for this study (Fig. 1a) far from the open boundaries. Initial and boundary conditions were obtained from the MFS (Mediterranean Forecasting System) regional model (Pinardi et al., 2003). MFS model temperature, salinity, current and sea surface elevation, provided every 24 h with a 1/16° (5–7 km) resolution, were interpolated on the MENOR grid. Atmospheric forcing was obtained from a MM5 model every 3 h. MARS3D for the NW Mediterranean has been operational since the beginning of 2005 in the framework of the MOON project (<http://www.moon-oceanforecasting.eu>), producing 3-hourly simulations.

The validation of the MARS3D simulations for the years 2005–2006 was done for the Gulf of Lions by comparing the main characteristics of the simulated shelf-slope circulation with *in situ* and satellite observations in the framework of the ECOLOPHY project (André et al., 2005; André, 2007). On the whole, the seasonal variability of the circulation, described by a large scale cyclonic gyre over the north-western Mediterranean basin, was accurately reproduced in the simulations (André et al., 2005). In winter, the circulation is broad and intense due to winter convection. In summer, the circulation weakens and splits into two parts, with a main gyre in the middle of the Northern Basin and a smaller one north of the isle of Corsica. Offshore from the Gulf of Lions, the velocity of the modelled NC was in the range of 0.25 m/s at the end of summer and 0.50 m/s during winter. The water vein was about 30–50 km wide, with the current flowing at the top of the slope. In agreement with *in situ*

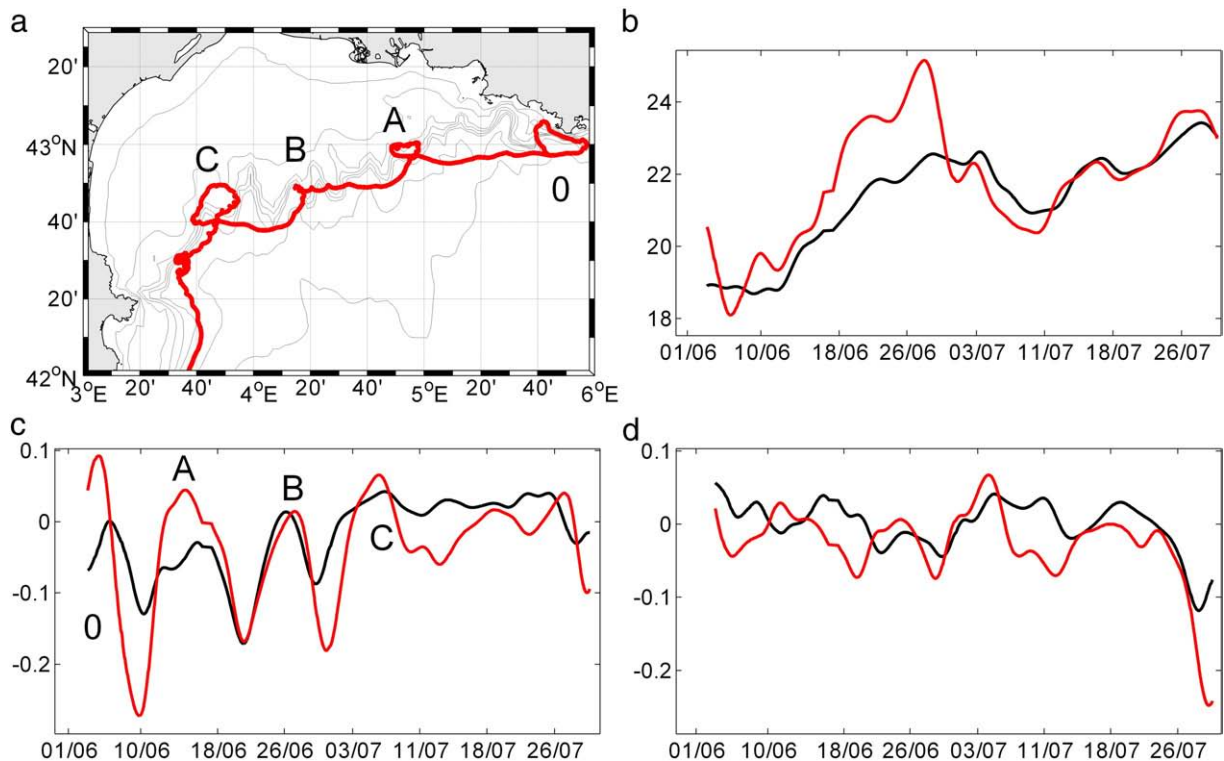


Fig. 3. a) Trajectory of buoy 61295 launched on 30 May off Toulon (isobath marks 200 m depth). b) Surface temperature in °C along the trajectory of buoy 61296 given by the surface float temperature sensor (red line) and extracted from numerical simulations at the corresponding positions in time (black line). c) Zonal velocities (m/s) at 50 m depth along the buoy trajectory derived from successive observed buoy positions (red line) and extracted from model simulations (black line). d) Meridional velocities (m/s) at 50 m depth along the buoy trajectory derived from successive observed buoy positions (red line) and extracted from model simulations (black line).

measurements (and also with climatology data), the maximum velocity was reached at subsurface level and the vertical extension of the current was about 600 m (not shown). At mesoscales, the meanders and eddies of the NC are noticeable both in the modelled fields and on SST imagery, showing similar length scales (André et al., 2005).

Although the simulations and the reality agreed significantly in qualitative and quantitative terms, the model was not expected to be able to exactly reproduce the trajectories of the drifters launched in the NC vein. Nevertheless, the comparison of modelled and measured physical quantities along the trajectory of one of the ECOLOPHY buoys is given as an example, in Fig. 3. As seen in this figure, drifter 61295 launched offshore of Toulon on 30 May followed the upper slope for several weeks, leaving the vein of the NC on four occasions to circulate in four different mesoscale structures over the shelf break (Fig. 3a). The first one, off Toulon (named eddy 0; 5.5°E; 2–4 June) appeared over the shelf as consequence of a local upwelling. The second (eddy A; 5.0°E; 15 June), the (small) third (eddy B; 4.3°E; 26 June) and the fourth (eddy C; 3.8°E; 5 July) were located over the upper slope. The comparison between observed (Lagrangian) and model (Eulerian) velocities (also low-pass filtered at a cut-off period of 18 h) along the track of the buoy (i.e. at each position and time) showed significant agreement, for instance, when the buoy was advected by the NC between eddy A and eddy B, with modelled and observed velocities in the range of 0.30 m/s. Stronger model-data discrepancies were found over the slope in the sections of the trajectory between eddy B and eddy C and, specifically, between eddies 0 and A. In the latter case, the model current was weaker (0.10 m/s) than the observed one (0.25 m/s), as the modelled NC was wrongly positioned locally (too far south). Comparison of model and observed velocities when the buoy was circulating in the four mesoscale eddies also showed good agreement in terms of the intensity and main orientation of the velocity field over the shelf. As for surface temperatures, despite the poor simulation of the sea surface overheating during a long period of very calm weather (19–29 July), the surface thermal patterns highlighted by observations were correctly reproduced in the simulations (Fig. 3b). Overall, this model-data comparison shows that MARS3D is able to reproduce the main characteristics of the Gulf of Lions shelf-slope circulation. However, as we will see below, the simulations did have noteworthy errors in terms of position, intensity and persistence of the NC mesoscale meanders and eddies.

3.2. Methodology for the reconstruction of Eulerian fields

The basic idea of the reconstruction procedure used in this study was to provide more realistic model coastal flows which potentially contain phase errors, i.e. velocity structures that are shifted over space and/or in time. Taking the observed drifter tracks, the local velocity field following each drifter's path was to be reconstructed within some correlation scales in order to improve the realism of the simulations.

The methodology, described in detail in Taillandier et al. (2006), consists in providing sequential velocity estimations with a fixed spatial scale R (related to the spatial length of the Eulerian field to be analysed) around simulated trajectories. For each sequence $[t_0, t_0 + \tau]$, a time-independent correction $\Delta \mathbf{u}$ is added to the time-dependent velocity field $\mathbf{u}(t)$ to provide an estimation $\mathbf{u}^{\text{est}}(t)$ over a characteristic time scale T (related to the time scale of the Eulerian field to be analysed), as:

$$\mathbf{u}^{\text{est}}(t) = \mathbf{u}(t) + \Delta \mathbf{u}, \quad t \in [t_0 - 1/2(T - \tau), t_0 + 1/2(T + \tau)] \quad (1)$$

where τ is related to the time scale of the Lagrangian data set. This velocity estimation ($\mathbf{u}^{\text{est}}(t)$) minimises the distance between trajectories simulated inside the velocity field $\mathbf{u}(t)$ and observed positions

\mathbf{r}^{obs} . For each sequence $[t_0, t_0 + \tau]$, this prediction misfit is expressed in the least square sense by the cost function:

$$J = 1/2 \left(\mathbf{r}^{\text{obs}}(t_0 + \tau) - \mathbf{H}_{\text{NL}}(\mathbf{u}) \right)^T \cdot \left(\mathbf{r}^{\text{obs}}(t_0 + \tau) - \mathbf{H}_{\text{NL}}(\mathbf{u}) \right) \quad (2)$$

where T denotes the vector transpose, whose components are assumed to be independent and associated with Gaussian homogeneous errors. The observational operator $\mathbf{H}_{\text{NL}}(\mathbf{u})$ provides position prediction at time $t_0 + \tau$ using trajectory simulations by the non linear equation:

$$d_t \mathbf{r} = \mathbf{u}(\mathbf{r}(t), t), \quad t \in [t_0, t_0 + \tau] \quad \text{with} \quad \mathbf{r}(t_0) = \mathbf{r}^{\text{obs}}(t_0) \quad (3)$$

where d_t is the first order derivative in time. The minimisation of J is performed by the steepest descent procedure along its gradient.

Each velocity correction $\Delta \mathbf{u}$ is specified by its spatial correlation structure, associated with a specific motion scale (R, T), using background error correlations explicitly included in the expression of the gradient of the cost function J (see details in Taillandier et al., 2006). In practice, this structure can be modelled by solving a diffusion equation over a length scale R , which interprets the spatial auto-covariance for the zonal or the meridional velocities (Derber and Rosati, 1989). Moreover, this sort of Laplacian grid-point smoother can account for anisotropic correlations which are inherent to the description of coastal flows, and imposed by the presence of coastlines (Weaver and Courtier, 2001).

3.3. Lagrangian diagnostics

The Eulerian description given by the simulated velocity fields can be assessed quantitatively by two Lagrangian diagnostics. Both involve simulated buoys drifting in time-varying velocity fields extracted from model outputs at 50 m (hereafter called “background fields”) or reconstructed from the combination of background fields and observed trajectories (hereafter called “reconstructed fields”). In numerical practice, simulated trajectories are computed offline using a fourth order Runge–Kutta scheme of 3 h-resolution and Lagrangian velocities provided by a bicubic interpolator.

The first diagnostic was designed to quantify the prediction error of the observed trajectories by the model. The evolution of the distance between observed drifter positions \mathbf{r}^{obs} and simulated drifter positions \mathbf{r}^{sim} is performed from a large set of initial conditions to:

$$e(\tau) = | \mathbf{r}^{\text{obs}}(t_0 + \tau) - \mathbf{r}^{\text{sim}}(t_0, t_0 + \tau) |, \quad \text{with} \quad \mathbf{r}^{\text{sim}}(t_0, t_0) = \mathbf{r}^{\text{obs}}(t_0) \quad (4)$$

where $\| \cdot \|$ measures the distance averaged over the different t_0 , taken at each available observed position value. This diagnostic was to be used as an indicator of the quality of the model field correction made through the variational analysis. As shown below, the prediction error made it possible to obtain the best parameterisations for reconstruction of the Eulerian fields.

A second diagnostic aimed to quantify the fate of water parcels advected by the NC, across the shelf slope. It was to provide quantitative assessments of residence times and water renewal in the gulf. To that end, a similar approach to that used in Veneziani et al. (2007) was set up: concentration maps from two different sources were provided and probability density functions were computed over the Gulf of Lions extension, binned at a 0.1° resolution. The first source was a simulated deployment involving 120 virtual drifters over the slope from 3.4 to 5.4 °E and the second source involved 45 virtual drifters regularly released over the shelf between 50 and 200 m

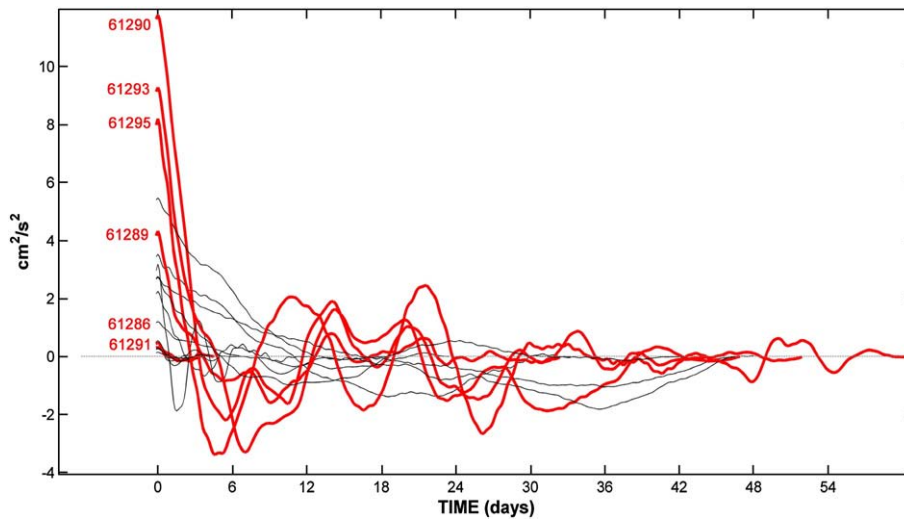


Fig. 4. Autocorrelation functions calculated for the along-slope component of the velocity along each trajectory described by June 2005 drifters in the Gulf of Lions. The 6 trajectories used for the reconstruction are plotted in red.

isobaths, from 3.4 to 5.4 °E. These simulated deployments were performed every 3 h over the time slot of interest. Then, concentration maps gave the percentage of trajectories (over the total number of trajectories within the domain represented in Fig. 1a) per bin resulting from the average over the set of deployments. Finally, in order to quantify the impact of the flux reconstruction at the coastal/offshore interface, the trend of the concentration of trajectories in two regions on the Gulf of Lions shelf (the north-eastern and the south-western shelves, shown in Fig. 1a) was computed over the period of interest.

4. Reconstruction of the Gulf of Lions shelf-slope circulation

The method presented in the previous section was then applied to the case of the NC. This required setting up specific parameterisations on the basis of information about the NC fluctuations' spatial (R) and time scales (T, τ).

4.1. Parameterisations

Lagrangian statistics were computed in order to obtain the scales characterising the Lagrangian data set. The statistics were calculated along the first 25 days of low-pass filtered velocity time series which corresponded to positions within the Gulf of Lions. To do so, both components of the velocity field had previously been rotated 20° counter-clockwise to align one of them with the main orientation of the slope current.

Following Poulain and Niiler (1989), the Lagrangian autocorrelations were calculated for the along- and cross-slope directions using Lagrangian residual velocities. An approximation of the first maximum of the integral Lagrangian time (τ) scale was obtained by

Table 1 Space and time scales used for the reconstruction procedure.

Lagrangian time scale (τ)	1 day
Eulerian time scale	
T _{inshore}	3.5 days
T _{offshore}	1.75 days
Spatial correlation	
R _{inshore}	10 km
R _{offshore}	10 km

Note the different Eulerian time scales used for the inshore/offshore analysis.

integrating the normalised Lagrangian autocorrelation functions from zero to the time of their first zero crossing.

The global data set shows a mesoscale signal with a time scale τ of around 2 days in the along-slope direction and 1 day in the cross-slope direction. The autocorrelation functions for the along-slope component of the velocity along each individual trajectory are shown in Fig. 4. Individual autocorrelations show two different regimes of trajectories. An initial regime corresponds to trajectories that followed the offshore side of the NC without exhibiting mesoscale patterns and presented non looping autocorrelation curves (see trajectories and autocorrelation curves depicted in grey in Figs. 1b and 4). The second regime corresponding to trajectories which circulate on the inshore side of the NC, occasionally leaving the NC's vein to circulate in mesoscale eddies over the shelf slope, showed strongly fluctuating autocorrelation curves (see trajectories and autocorrelation curves shown in red in Figs. 1b and 4). As we will see in the next subsection,

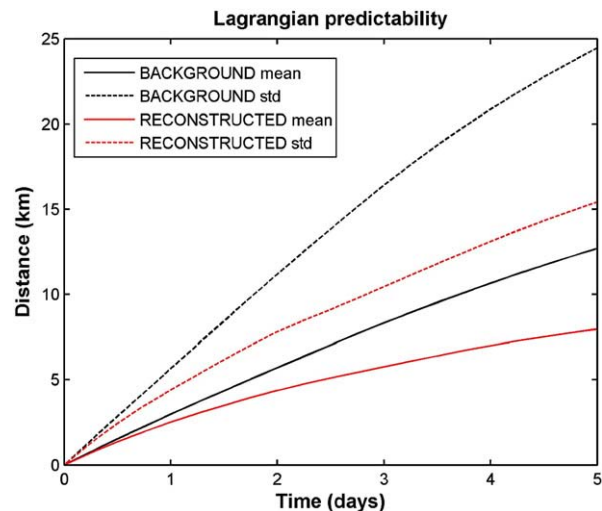


Fig. 5. Evolution of the Lagrangian predictability for background (black) and reconstructed (red) fields during the first 5 days of the analysis. The Lagrangian predictability was computed as the mean difference between observed positions and the set of estimated positions given by the virtual numerical drifters launched at each run. Dotted lines represent the standard deviations associated with these means.

the latter was the case of the trajectories chosen for the reconstruction. This set of trajectories gives an optimal scenario for the reconstruction, as it contains information about the current as well as the mesoscale structures present on the shelf slope.

The first approximation of the lower and higher values for the Eulerian spatial and temporal scales to be fixed when applying the reconstruction procedure can be directly obtained from the velocity fields given by model simulations. To estimate the Eulerian spatial scale (R) from the simulations, the correlation of every grid point with the rest of the others was calculated for the model velocity at each time step. Then a Gaussian function was adjusted to the spatial distribution of correlations (setting a maximum correlation radius of 50 km and a minimum correlation index of 0.7) to obtain an estimation of the correlation radius (R). The spatial distribution of the correlation radius showed values of around 10–15 km over the shelf, one area of small correlations over the upper slope ($R \sim 5$ km), and then values around 10–20 km over the slope and open sea (not shown). For the Eulerian time scale (T) the autocorrelation through the simulated period was computed for each component of the velocity at each grid point. Eulerian time scales (T) of fewer than 2 days were obtained over the shelf and slope and values between 2 and 6 days were observed in the open sea (not shown).

In addition, the shape of the NC and its variability seemed to involve frontal dynamics setting a dynamical barrier along the inshore edge of the coastal current and isolating the velocity correlations on each side. Consequently, two distinct regimes can be considered separately, one over the shelf and one offshore. These two regions are separated by a 25 km band located over the shelf slope which allows a progressive shift (values of α in Eq. (5) go gradually from 0 to 1) from one regime to the other. Hence, two distinct velocity corrections can be provided by the method (Section 3.2), $\Delta \mathbf{u}^{\text{in}}$ inshore and $\Delta \mathbf{u}^{\text{off}}$ offshore. The velocity estimation, given by Eq. (1), is then refined to the relation:

$$\mathbf{u}^{\text{est}}(t) = \mathbf{u}(t) + \alpha \cdot \Delta \mathbf{u}^{\text{in}} + (1 - \alpha) \cdot \Delta \mathbf{u}^{\text{off}}, \quad t \in [t_0 - 1/2(T - \tau), t_0 + 1/2(T + \tau)] \quad (5)$$

where α is equal to 1 inside the gulf extension, and quickly tends to 0 if going offshore. So each selected motion scale, taken separately on the shelf and offshore, would be the only one corrected by the reconstruction. Considering Eq. (5), this overall estimation was superimposed on other motion scales which had been filtered out or which could not be directly described by Lagrangian data.

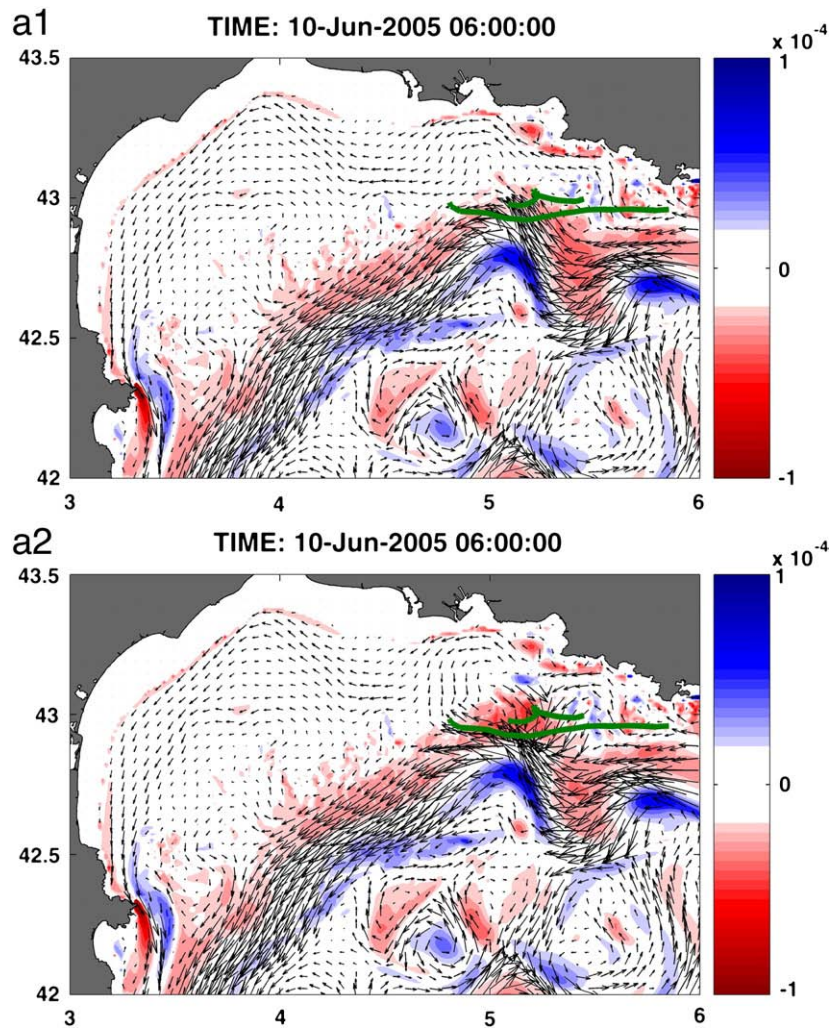


Fig. 6. Impact of the reconstruction of the Eulerian fields. a) 10 June background (top) and reconstructed (bottom) velocity (max velocities = 0.5 m/s) and relative vorticity fields (color bar units s^{-1}). Green lines indicate the segments of the simultaneous trajectories that were used for the reconstruction (± 3 days around the date of the snapshot). b) Black lines show the numerical trajectories of a set of virtual drifters released in the background and reconstructed velocity fields every 2 h between 30 May and 10 July around 5.5°E and $42.6\text{--}43^\circ \text{N}$. Superimposed red points indicate the real positions of the 6 drifters that were used to carry out the reconstruction. Isobaths: 50, 200, 1000 and 2000 m.

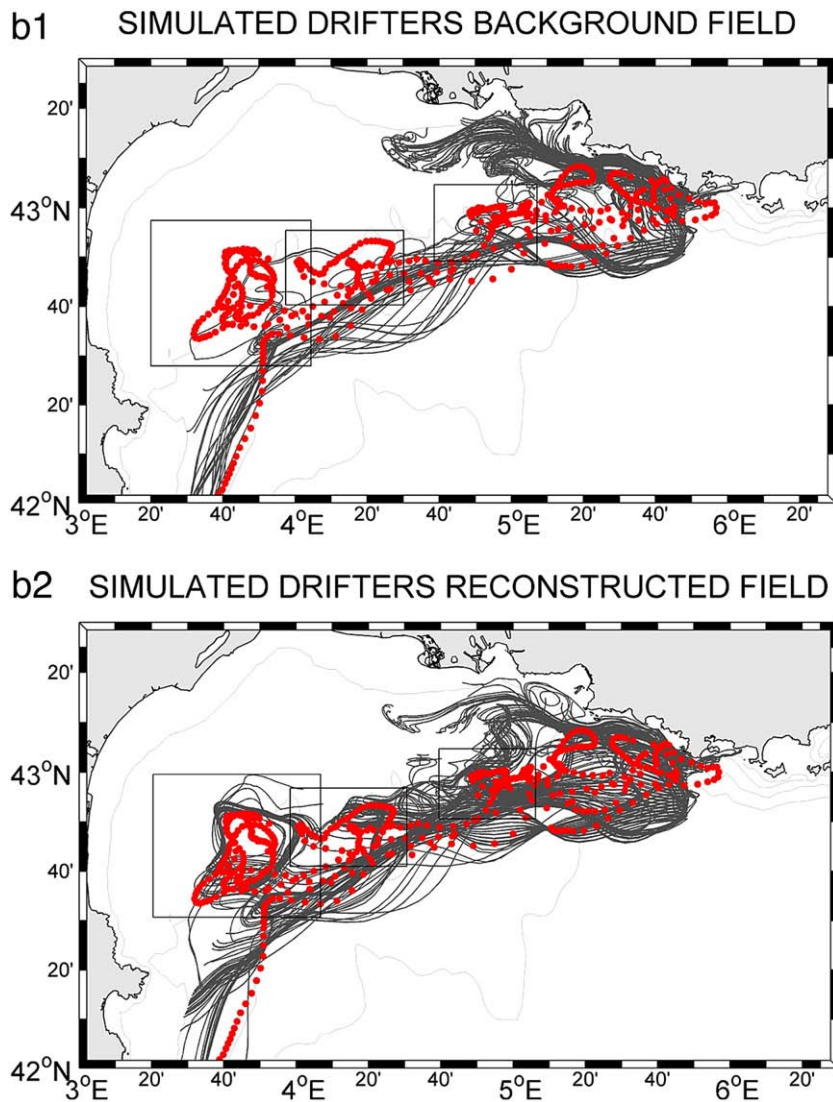


Fig. 6 (continued).

Several preliminary tests provided the reconstruction's sensitivity with respect to the choice of the Lagrangian and Eulerian space and time scales and the choice of the interface design separating the coastal and offshore zones. The efficiency of each run was assessed on the basis of the prediction error (given in detail in Section 3.3, Eq. (4)). The configuration which was selected (Table 1) is the one that minimises this criterion. The Lagrangian time scale was set to 1 day to ensure the good sampling of the mesoscale signal shown by the trajectories (1–2 days) and the spatial correlation to 10 km in both inshore and offshore regimes (consistent with the Eulerian scales characterising the simulated fields). Finally, the value of 1.75 days, chosen for the offshore Eulerian time scale, ensured good sampling of the rapidly evolving trajectories advected by the NC over the slope.

The prediction error for the selected configuration is represented in Fig. 5 and compared with the prediction error of the background fields. Both cases present exponential growth of the mean prediction error (mean error calculated for all runs) with this growth being slower for the reconstructed fields. As shown in the figure, in the first days after the release of the virtual buoys in each of the velocity fields, Lagrangian predictability is significantly improved by the reconstruction. If we consider the errors for the day 5 after the release of the

numerical drifters, the reconstruction helps decrease the prediction error from 12 to 8 km (i.e. by 30%).

4.2. Experimental set up

The configuration presented in the previous section was used to reconstruct Eulerian fields between 29 May and 10 July, 2005. To do so, the 6 trajectories marked in red in Fig. 1 (also see their autocorrelation functions in Fig. 4) were used in combination with the corresponding model-simulated fields. Trajectories inside the NC, which reveal intense meandering, provided corrections for the position, intensity and width of the model-simulated NC. Trajectories which sampled the mesoscale activity over the shelf were used to reorganize the model-simulated eddy activity by refining the location and shape of mesoscale eddies along the shelf slope.

The method was applied for an analysis of the trajectories during the successive sequences of duration τ covering the period of interest. The $\Delta \mathbf{u}$ correction was computed with respect to the mesoscale velocity field extracted from MARS model outputs at 50 m. The assimilation procedure was performed offline. This avoids any propagation by model dynamics of velocity shift corrections, or any

adjustment of other model errors (directly linked to boundary conditions, forcing or parameterisation). Even if the data coverage is uniform over the period of analysis (Fig. 2), the reconstruction of the flow field will only be patchily effective over the study area. On the

other hand, assuming that the method is implemented in an operational system, this data density would be sufficient to carry out the reconstruction of the mesoscale NC fluctuations during the period.

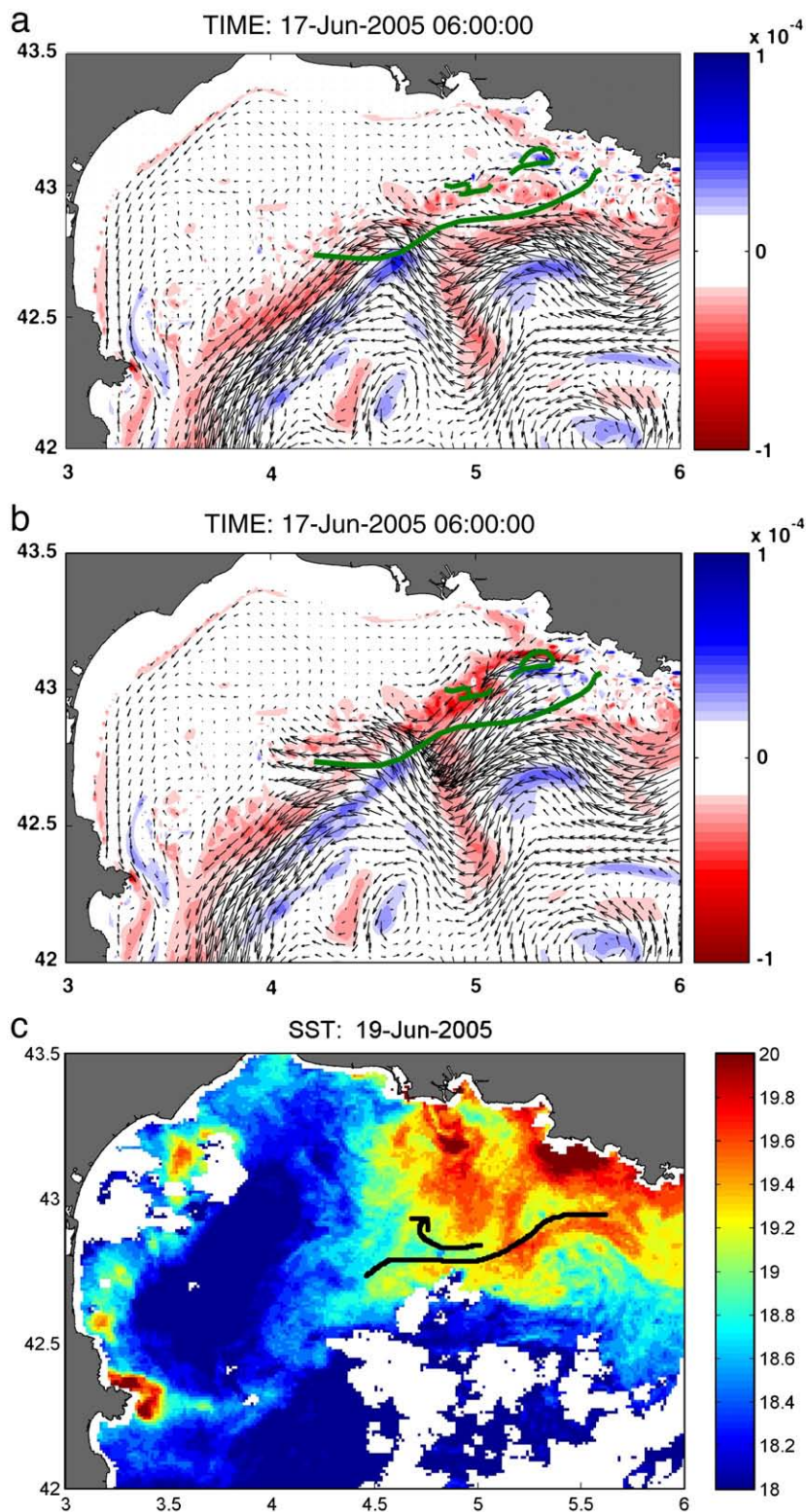


Fig. 7. 17 June background (a) and reconstructed (b) velocity (max velocities = 0.5 m/s) and relative vorticity fields (color bar units s^{-1}). Green lines indicate the segments of the simultaneous trajectories that were used for the reconstruction (± 3 days around the date of the snapshot). (c) SST image for 19 June (color bar units $^{\circ}\text{C}$). Black lines indicate the position of eddy A, inferred from the SST.

5. Results

The impact of the reconstruction was assessed by a qualitative comparison of background and reconstructed fields. Next, by comparing the reconstructed fields with contemporary SST images it was possible to describe the mesoscale field and, at the same time, to validate the results of the reconstruction. Finally, the background and reconstructed fields were used to perform comparative Lagrangian diagnostics on the Gulf of Lions shelf-slope transports.

5.1. Impact of the reconstruction

As an example, the background and reconstructed velocity and relative vorticity fields for 10 June are compared in Fig. 6a. The relative vorticity derived from the velocity field helps describe the mesoscale patterns present in these fields and get a clearer comparison between them. As explained in the previous section, the reconstruction was done using a sequential method and thus its impact is limited over time and space around the area where the real trajectories were located. On 10 June, the Eulerian field was corrected using two trajectories located in the NE of the Gulf of Lions (see green lines in

Fig. 6a). The effects of the reconstruction can be observed in this zone where the relative vorticity shows a well-defined anticyclonic pattern (negative vorticity) in the inshore part of the NC, around 43.1°N 5.1°E , corresponding to eddy A (defined in Section 3.1). On this part of the slope, comparison of model background fields and the observed trajectories confirmed that the model NC was located too far offshore. Moreover, although NC meandering had real space and time scales, the model NC meanders were not placed in the right location. In fact, the local intensification of circulation around 43°N between 5 and 5.5°E in the reconstructed fields results from the correction of model velocity fields using these two trajectories which correspond to buoys within the NC vein (i.e. with high drifting velocities).

Through the period of interest, the sequential correction of model-observation misfits in terms of NC meanders and eddies improved the Lagrangian representation of circulation in the area. This is clear when both fields are compared through the trajectories of numerical drifters (Fig. 6b) released around 5.5°E and 42.5 – 43.1°N in the background and reconstructed velocity fields every 6 h during the period of interest. Differences between these two sets of trajectories were mainly significant along the shelf border in the cases of eddies B and C. As shown in Section 3.1, the model was able to correctly represent

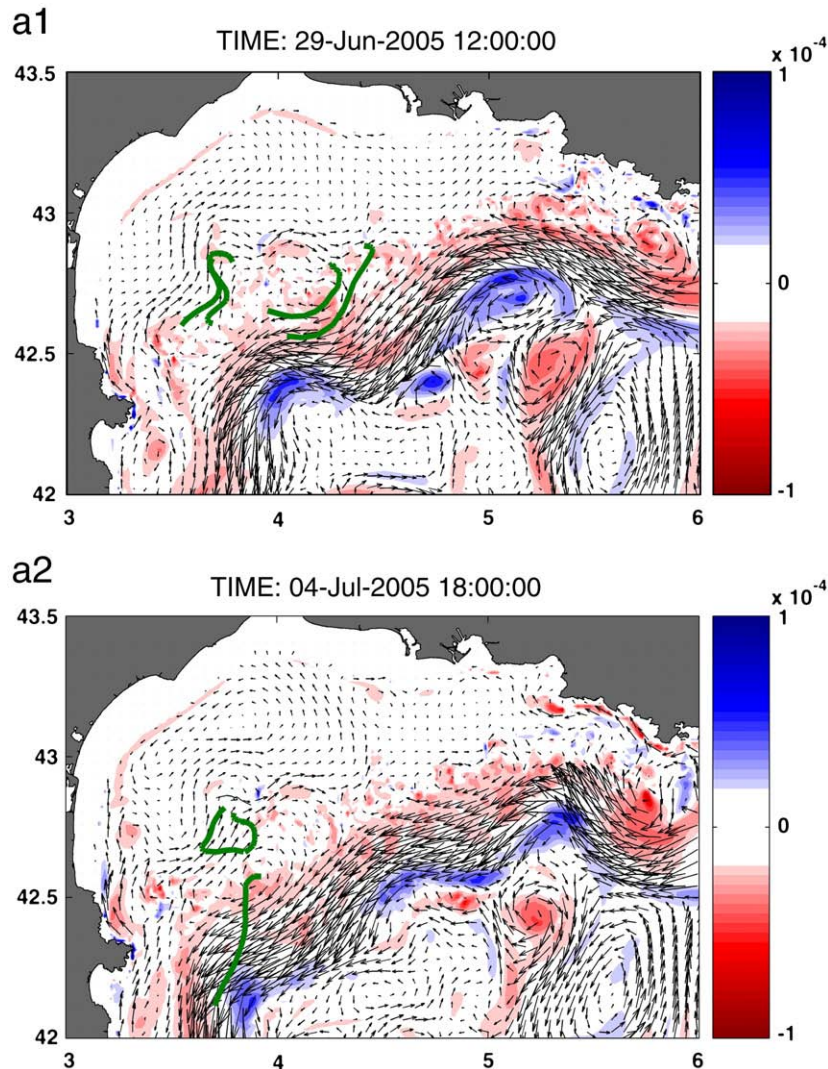


Fig. 8. 29 June (top) and 4 July (bottom) background (a) and reconstructed (b) velocity (max velocities = 0.5 m/s) and relative vorticity fields (color bar units s^{-1}). Green lines indicate the segments of the simultaneous trajectories that were used for the reconstruction (± 3 days around the date of the snapshot). (c) SST images for (top) 29 June and (bottom) 5 July (color bar units: $^{\circ}\text{C}$). Black lines indicate the position of eddy C, inferred from SST.

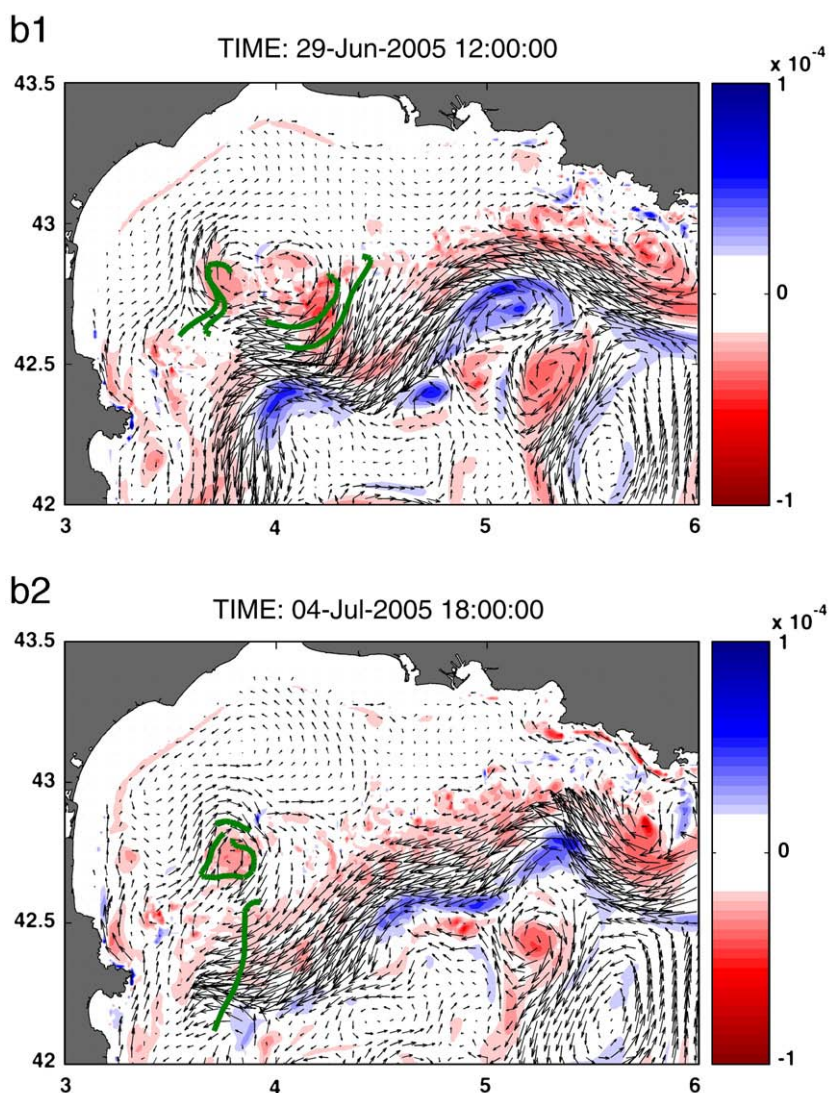


Fig. 8 (continued).

some of these mesoscale patterns, however the mesoscale activity was underestimated in the simulations.

5.2. Mesoscale structures and shelf-slope exchanges

Comparing the reconstructed Eulerian fields and information from contemporary SST imagery enabled the main characteristics of the three mesoscale anticyclonic eddies observed over the shelf slope during the period of interest to be described. In all cases, eddies were closely related to the meandering of the NC and located on its coastal side. Eddy A, observed by two trajectories between 10 and 17 June, had mean velocities around 0.3 m/s. Reconstructed fields and SST images for 10 June suggest that this eddy's diameter was about 25 km and that it was associated with an NC meander with a wavelength of 40 km. Although the model fields showed the meandering of the NC, eddy A was not present in the simulations for 10 June. In the reconstructed fields for 17 June (Fig. 7b), eddy A had moved south-westwards to 4.8°E and 42.9°N and showed a larger diameter (~40 km). In this case, it could also be observed in the background of the model fields (shown up by a slight negative vorticity patch around 4.9°E and 42.9°N) although the velocity field associated with the eddy was much weaker (Fig. 7a). Model NC was located too far offshore and the NC meander was time-shifted. The reconstruction repositioned the

meandering and intensified the circulation around 5–5.5°E and 43°N. The surface signal of eddy A in SST terms could be identified in the satellite image for 19 June (SST information for 17 & 18 June was not available due to cloud coverage) where the meandering of the NC was also well defined (Fig. 7c). Eddy B was revealed by two trajectories between 18 and 29 June around 42.8°N, 4.4°E (not shown). This eddy, with a diameter of approximately 25 km, was observed drifting south-westward with the NC meandering until 29 June, when it merged with eddy C, reinforcing the latter structure. Eddy C was observed from 23 June to 12 July, by three drifter trajectories over the shelf. Based on reconstruction and SST fields, this eddy's diameter was between 30 and 40 km. Eddy C remained in the same position over the Boucart submarine canyon (3.7°E, 42.7°N) throughout the observation period, suggesting that it had a deep structure and interacted with the bathymetry. The surface signal of this eddy clearly appears in the SST images on 29 June and 5 July with similar dimensions to those suggested by the reconstruction (Fig. 8c). For the same dates (Fig. 8a) the background fields show a clear anticyclonic pattern in the same area with a north-westerly current between 3.5 and 4°E and a westerly current between 4 and 4.4°E, in agreement with the circulation described by the real trajectories. However the model does not reproduce any eddy which was not in agreement with observations (Fig. 8a).

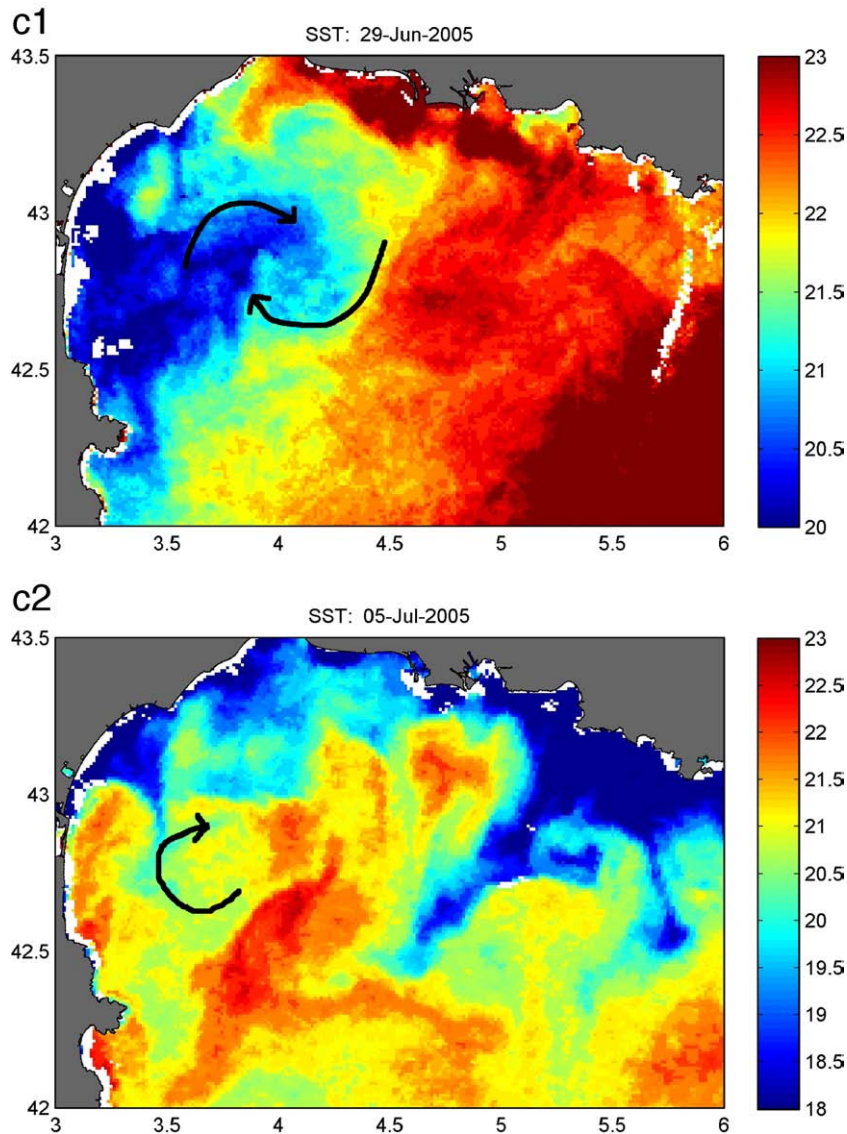


Fig. 8 (continued).

In order to study the effect of the reconstruction on the shelf-slope transport, differences between the background and reconstructed fields were analysed using density maps of concentrations of numerical trajectories, as described in Section 3.3. To illustrate the spatial distribution of the transports, the concentration maps are shown for the slope deployment (Fig. 9) 6, 18, 30 and 42 days after the virtual deployment (corresponding to 3, 15 and 27 June and 9 July). The concentration maps for the reconstructed fields (Fig. 9) show three zones of convergence of pathways associated with virtual drifters trapped within the 3 reconstructed eddies described above. The qualitative comparison of reconstructed and background distributions showed significant differences in terms of trajectory transports from the slope to the shelf. Between two and three weeks after the deployment, the main differences between the background and reconstructed fields can be observed in the north-easternmost part of the Gulf of Lions, mainly between 4.5° and 5.8°E, since the real drifters had not yet covered other areas in the gulf. Higher concentrations could be observed in the reconstructed fields around eddy A on the successive distributions up to 30 June, in agreement with the lifetime of the eddy. In contrast, the maps for the background model fields show higher concentrations at the entrance of the Gulf, over the shelf slope in front of Marseille coast. The distribution of the reconstructed fields on 27 June displayed two main

points of convergence associated with eddies B and C. The point of high concentrations around eddy B can be observed from 17 to 27 June and that around eddy C can be observed until the end of the period. In the background fields, these two maxima are not present. However, high concentration values are observed in the south-western part of the slope, associated with the anticyclonic patterns shown by the simulations over the shelf. With time, the number of trajectories moving from the slope to the NE shelf was larger for the reconstructed fields by 6% from 6 to 14 June associated with eddy A, and by 10% from 18 to 28 June associated with eddy B. In contrast, from early July to the end of the period, the percent of trajectories in the NE shelf was around 5% lower than in the background field. The latter difference seems to be linked to higher transports (in the reconstructed fields) from the NE shelf to the SW shelf and the strong accumulation of trajectories around eddy C on the SW shelf. On the SW shelf, strong differences between the background and reconstructed fields were obtained between 21 June and 3 July, associated with eddy C. During this period, transports from the slope (and also in part from the NE shelf) to the SW shelf increased by about 15–20% in the reconstruction.

The shelf deployments evidence the same three points of convergence (associated with eddies A, B and C) in the reconstructed fields (not shown). The greatest differences between background and

reconstructed fields were obtained on the NE shelf, from 27 June to 9 July, with the concentration over the north-eastern shelf being 20% lower for the reconstructed fields. This seems to result from the combined effect of increased cross-slope transport associated with eddies A and B in the NE part and trajectories imported from the NE to the SW part of the shelf. In the SW part of the shelf, the strongest concentration around eddy C was balanced by increased transport from shelf to slope. Export of trajectories from shelf to slope, over the entire shelf (NE + SW), rose by 25% in the reconstructed fields. For example, in the map for 9 July (not shown) 77% of trajectories remained over the shelf in the case of background fields, while only 52% of the trajectories remained over the shelf for the reconstructed field.

6. Summary and concluding remarks

The reconstruction of the along-slope circulation in the Gulf of Lions was carried out using an inverse method which combines Lagrangian observations of the NC with the outputs of a hydrodynamic numerical model for the NW Mediterranean. Along-slope Lagrangian observations were obtained through the regular deployment of satellite tracked drifters in the vein of the NC in the upstream limit of the Gulf of Lions. The drifters, anchored at 50 m to ensure their free

drift over the deeper parts of the Gulf of Lions' shelf to match the currents under the Ekman layer, provided valuable information on the NC mesoscale variability. Comparison of drifter trajectories with model outputs showed that simulations reproduce the main characteristics of slope circulation but that there are also significant errors concerning the position, size and persistence of model mesoscale structures associated with the NC over the shelf slope. The reconstruction of simulated fields using the observed trajectories enables model errors to be corrected and gives a more realistic description of the shelf-slope mesoscale dynamics. Quantitative Eulerian validation of the results presented here was not possible due to the lack of an adequate set of observations along the Gulf of Lions shelf slope. Complementary in-situ Eulerian observations available for these dates from the ECOLPHY French campaigns (see André, 2007), only covered a limited region over the slope area at the entrance of the Gulf of Lions (to the east of 5°E) not allowing a quantitative validation of our analysis. Other possibilities, such as the use of altimeter data, were disregarded due to the significant errors of altimeter measurements near the coast and to their low time/space resolution. However, we would like to note that quantitative comparisons were made while testing several different configurations of the reconstruction methodology (which did not always use all available Lagrangian data), by comparing the

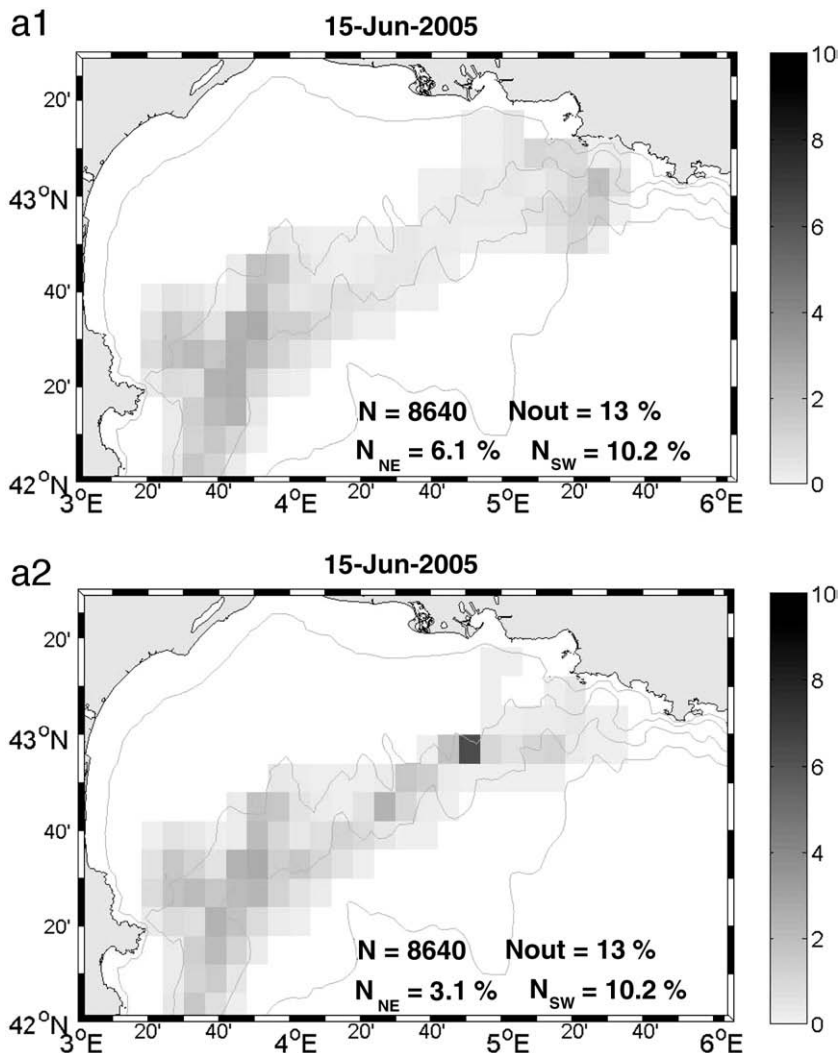


Fig. 9. Concentration maps obtained as a result of the release of numerical drifters over the slope in background (top) and reconstructed (bottom) velocity fields. The color bar represents the percentage of trajectories (over the total number of trajectories N within the area of interest) per bin resulting from the average over the set of runs. For clarity, values over 10% have been set to 10%. N is the number of trajectories within the study area, N_{out} is the percent of trajectories that have left the area (i.e. buoys that had crossed the southern limit of 42°N) at the moment represented by the figure. N_{NE} and N_{SW} are the percents of drifters within the NE and SW parts of the shelf, respectively. Isobaths: 50, 200, 1000 and 2000 m.

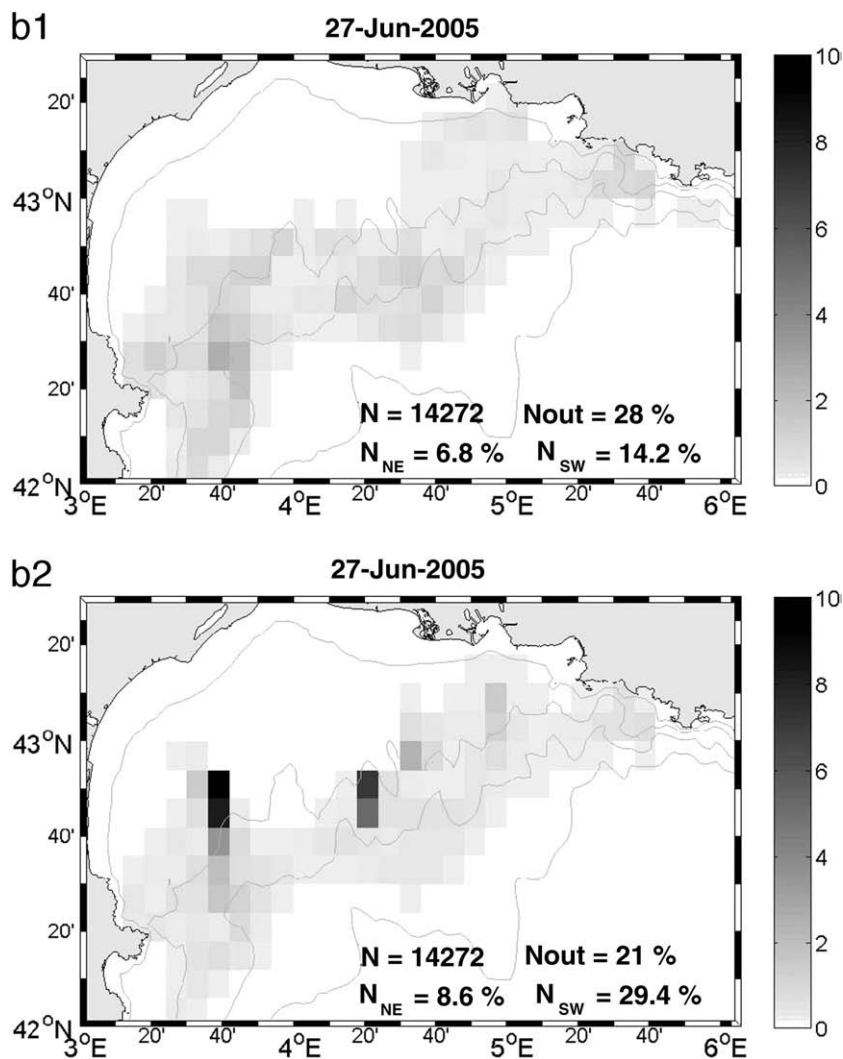


Fig. 9 (continued).

Eulerian results with the remaining trajectories. These comparisons, together with the minimisation of the Lagrangian predictability errors, enabled the different parameterisations for the reconstruction to be validated.

Comparison of reconstructed fields, observed trajectories and satellite imagery focused on mesoscale eddies present during the period of interest. Reconstructed eddies, their main characteristics and dynamics are in agreement with previous observations (Flexas et al., 2002; Rubio et al., 2005, 2007). That is to say that three anticyclonic eddies with diameters from 20 to 40 km were observed in the inner (inshore) part of the NC. Two of them were observed to drift south-westerly in association with the NC meandering along the slope, while the third seemed to interact with the bathymetry, since it remained above the head of a submarine canyon during the period of study. The comparison, performed in terms of integrated transport of virtual drifters released in background (simulated) and reconstructed fields allowed the impact of the reconstruction to be evaluated. Moreover, the comparative analysis of these two fields provided insight on the effect of NC mesoscale variability on the shelf-slope exchanges in the Gulf of Lions. As an overall result, shelf-slope transports in the gulf were significantly enhanced when the reconstruction was applied to model simulations. This result was expected, since the comparison between modelled and observed trajectories has shown that the circulation model tends to underestimate mesoscale variability

over the shelf slope, giving a partial representation of the observed mesoscale features.

Finally, it is worth noting that the methodology used in this work can be applied to issues related to Rapid Environmental Assessment. Operational systems devoted to ocean forecasting are expected to give rapid and accurate responses for the management of marine environmental problems, like those related to the drift of marine pollutants in coastal areas. Nevertheless, simulations of the highly complex coastal hydrodynamic conditions by these modelling systems usually contain unavoidable errors due to various issues such as the unresolved physics, limitations on time and space resolution or incomplete knowledge of the forcings. This paper describes improvement in the performance of one of these oceanographic operational systems in a coastal area, using a simple reconstruction procedure fed by a reduced set of in-situ Lagrangian observations.

Acknowledgements

The work of A. Rubio was funded in part by the Provence Cote d'Azur Regional Council. V. Taillandier received funding from ANR (LIVINGSTONE project). A. Rubio and P. Garreau thank D. Sauzade, A. Petrenko, A. Doglioli and G. Jordà for their help and their useful comments. A. Rubio would like to thank PRECARIOS, a postgraduate

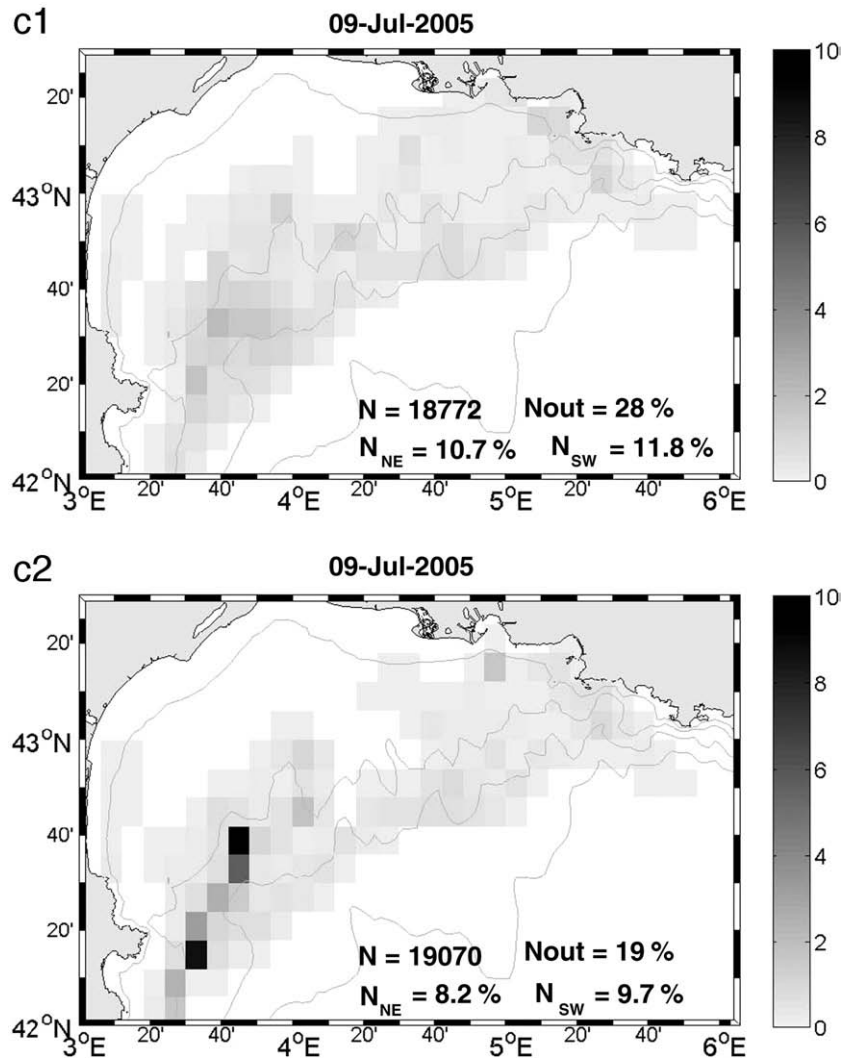


Fig. 9 (continued).

organisation whose dedication and efforts contribute to improving the working conditions for young scientists in Spain (www.Precarios.org).

References

- Alberola, C., Millot, C., Font, J., 1995. On the seasonal and mesoscale variability of the Northern Current during the PRIMO-0 experiment in the western Mediterranean Sea. *Oceanol. Acta* 18 (2), 163–192.
- André, G., 2007. Echanges côte-large à moyenne échelle au niveau de la pente continentale du Golfe du Lion. *Processus et Modélisation*. PhD thesis, Université de Toulon et du Var. 209 pp.
- André, G., Garreau, P., Garnier, V., Fraunié, P., 2005. Modelled variability of the sea surface circulation in the North-western Mediterranean Sea and in the Gulf of Lions. *Ocean Dyn.* 55, 294–308.
- Arakawa, A., Lamb, V.R., 1977. Computational design of the basic dynamical processes of the UCLA general circulation model. General circulation models of the atmosphere. In: Chang, J. (Ed.), *Methods in Computational Physics: Advances in Research and Applications*. Academic Press, San Francisco, pp. 173–265.
- Castellari, S., Griffa, A., Özgökmen, T.M., Poulain, P.M., 2001. Prediction of particle trajectories in the Adriatic Sea using Lagrangian data assimilation. *J. Mar. Syst.* 29, 33–50.
- Conan, P., Millot, C., 1995. Variability of the northern current off Marseilles, western Mediterranean Sea, from February to June 1992. *Oceanol. Acta* 18 (2), 193–205.
- Crépon, M., Wald, L., Monget, M., 1982. Low-frequency waves in the Ligurian Sea during December 1977. *J. Geophys. Res.* 87 (C1), 595–600.
- Davis, R.E., 1991. Observing the general circulation with floats. *Deep-Sea Res.* 38 (1), 531–571.
- Derber, J., Rosati, A., 1989. A global oceanic data assimilation system. *J. Phys. Oceanogr.* 19 (9), 1333–1347.
- Durrieu de Madron, X., Radakovitch, O., Heussner, S., Loye-Pilot, M.D., Monaco, A., 1999. Role of the climatological and current variability on shelf-slope exchanges of particulate matter. Evidence from the Rhône continental margin (NW Mediterranean). *Deep-Sea Res.* 46, 1513–1538.
- Flexas, M.M., Durrieu de Madron, X., Garcia, M.A., Canals, M., Arnau, P., 2002. Flow variability in the Gulf of Lions during the Mater HFF Experiment (March–May 1997). *J. Mar. Syst.* 33–34, 197–214.
- Flexas, M.M., van Heijst, G.J.F., Trieling, R.R., 2005. The behavior of jet currents over a continental slope topography with a possible application to the Northern Current. *J. Phys. Oceanogr.* 35, 790–810.
- Kamachi, M., O'Brien, J.J., 1995. Continuous assimilation of drifting buoy trajectories into an equatorial Pacific Ocean model. *J. Mar. Syst.* 6, 159–178.
- Kuznetsov, L., Ide, K., Jones, C.K.R.T., 2003. A method for assimilation of Lagrangian data. *Mon. Weather Rev.* 131, 2247–2260.
- Lazure, P., Dumas, F., 2008. An external-internal mode coupling for a 3D hydrodynamical model for applications at regional scale (MARS). *Adv. Water Resour.* 31 (2), 233–250.
- Lopez z-Garcia, M.J., Millot, C., Font, J., Garcia-Ladona, E., 1994. Surface circulation variability in the Balearic Basin. *J. Geophys. Res.* 99 (C2), 3285–3296.
- Millot, C., 1990. The Gulf of Lions' hydrodynamics. *Cont. Shelf Res.* 10 (9–11), 885–894.
- Millot, C., 1999. Circulation in the Western Mediterranean Sea. *J. Mar. Syst.* 20, 423–442.
- Molcard, A., Piterberg, L.I., Griffa, A., Özgökmen, T.M., Mariano, A.J., 2003. Assimilation of drifter positions for the reconstruction of the Eulerian circulation field. *J. Geophys. Res.* 108 (3), 3056.
- Özgökmen, T.M., Griffa, A., Piterberg, L.I., Mariano, A.J., 2000. On the predictability of the Lagrangian trajectories in the ocean. *J. Atmos. Ocean. Technol.* 17, 366–383.
- Özgökmen, T.M., Molcard, A., Chin, T.M., Piterberg, L.I., Griffa, A., 2003. Assimilation of drifter positions in primitive equation models of midlatitude ocean circulation. *J. Geophys. Res.* 108 (C7), 3238.
- Pinardi, N., Allen, I., Demirov, E., De Mey, P., Korres, G., Lascaratos, A., Le Traon, P.-Y., Maillard, C., Manzella, G., Tziavos, C., 2003. The Mediterranean ocean forecasting system: first phase of implementation (1998–2001). *Ann. Geophys.* 21, 3–20.

- Poulain, P.M., 2001. Adriatic sea surface circulation as derived from the drifter data between 1990 and 1999. *J. Mar. Syst.* 29, 3–32.
- Poulain, P.-M., Niiler, P.P., 1989. Statistical analysis of the surface circulation in the California current system using satellite-tracked drifters. *J. Phys. Oceanogr.* 19, 1588–1603.
- Rixen, M., Ferreira-Coelho, E., 2007. Operational surface drift prediction using linear and non-linear hyper-ensemble statistics on atmospheric and ocean models. *J. Mar. Syst.* 65 (1–4), 105–121.
- Rixen, M., Ferreira-Coelho, E., Signell, R., 2008. Surface drift prediction in the Adriatic Sea using hyper-ensemble statistics on atmospheric, ocean and wave models: Uncertainties and probability distribution areas. *J. Mar. Syst.* 69 (1), 86–98.
- Rubio, A., Arnau, P.A., Espino, M., Flexas, M., Jordà, G., Salat, J., Puigdefàbregas, J., S.-Arcilla, A., 2005. A field study of the behaviour of an anticyclonic eddy on the Catalan continental shelf (NW Mediterranean). *Prog. Oceanogr.* 66 (2–4), 142–156.
- Rubio, A., Espino, M., Barnier, B., Jordà, G., 2007. Mesoscale anticyclonic eddies in the Catalan Sea: origin and dynamics. *CIESM 38th Congress Proceedings. Int. Mer. Medit.*, vol. 38, p. 193.
- Salas, J., Millot, C., Font, J., Garcia-Ladona, E., 2002. Analysis of mesoscale phenomena in the Algerian basin observed with drifting buoys and infrared images. *Deep-Sea Res.* 1 49 (2), 245–266.
- Sammari, C., Millot, C., Prieur, L., 1995. Aspects of the seasonal and mesoscale variability of the Northern current in the western Mediterranean Sea inferred from the PROLIG-2 and PROS-6 experiments. *Deep Sea Res.* 1 42 (6), 893–917.
- Taillandier, V., Griffa, A., 2006. Implementation of position assimilation for ARGO floats in a realistic Mediterranean Sea OPA model and twin experiment testing. *Ocean Sci.* 2, 223–236.
- Taillandier, V., Griffa, A., Molcard, A., 2006. A variational approach for the reconstruction of regional scale Eulerian velocity fields from Lagrangian data. *Ocean Model.* 13 (1), 1–24.
- Testor, P., Gascard, J.C., 2003. Large-scale spreading of deep waters in the Western Mediterranean Sea by submesoscale coherent eddies. *J. Phys. Oceanogr.* 33, 75–87.
- Toner, M.S., Kirwan, A.D., Kantha, L.H., Choi, J.K., 2001. Can general circulation models be assessed and their output enhanced with drifter data? *J. Geophys. Res.* 106, 19563–19579.
- Veneziani, M., Griffa, A., Poulain, P.-M., 2007. Historical drifter data and statistical prediction of particle motion: a case study in the central Adriatic Sea. *J. Atmos. Ocean. Technol.* 24, 235–254.
- Weaver, A.T., Courtier, P., 2001. Correlation modelling on the sphere using a generalized diffusion equation. *Q. J. R. Meteorol. Soc.* 127, 1815–1846.